INVESTIGATION OF FLOW BOILING HEAT TRANSFER CHARACTERISTIC OF MIXTURE REFRIGERANT L-41B IN A HORIZONTAL SMOOTH TUBE

by

Jinyou QIU[a,b,c*], Yonglin FANG[a], Guilong DAI[a], Xiaoming CHEN[a], Hua ZHANG[b], Weidong WU[b], and Zhihon WU[c]

[a] Key Laboratory of New Energy and Energy-Saving in Building, Fujian University of Technology, Fuzhou, China
[b] School of Energy and Power Engineering, University of Shanghai for Science and Technology, Shanghai, China
[c] CSCEC Strait Construction and Development Co., Ltd, Fuzhou, China

Original scientific paper
https://doi.org/10.2298/TSCI180115154Q

The saturated flow boiling heat transfer characteristics of L-41b, R1234ze(E)/R32 (27/73 mass%), inside an 8 mm ID horizontal tube were investigated. The experiment were carried out at the saturation temperature of 10 to 20 °C with heat flux ranging from 5 to 10 kW/m^2 and mass flux ranging from 200-500 kg/m^{2}s. The influence of mass flux, heat flux, and quality on the heat transfer coefficients were examined and discussed. The experimental data of local heat transfer coefficients were compared with four well-known correlations available in literatures. Additionally, a new vapour-phase multiplier correlation to predict the local heat transfer coefficients of L-41b flow boiling inside smooth tubes was developed. The results show that the deviations of the new correlation are within –24.98% to +14.68% to the experimental data and that the 95% prediction values are within ±15%.

Key words: *R1234ze(E), L-41b, flow boiling heat transfer, correlation*

Introduction

As refrigerants, hydrofluorocarbons (HFC) are widely used in refrigeration and heat pump system. Although HFC are non-ozone depleting, they do have large global warming potential (GWP), which could lead to global warming [1, 2]. Looking for the proper low GWP alternative refrigerant is important and urgent for the refrigeration and air conditioning.

Recently, many alternative refrigerants were proposed, including low GWP HFC, natural refrigerants, and hydrofluoroolefins (HFO). However, these efforts still have not achieved satisfactory success, because rare pure refrigerants can completely meet the environmental, thermodynamic, and safety requirements of new-generation refrigerants [3].

In the recent years, HFO have attracted great attention because of the low GWP value. In particular, R1234ze(E) as a kind of HFO which was found to be low flammability, non-toxicity, zero ozone depletion potential (ODP) and quite low GWP (GWP < 1) [4]. The R1234ze(E) was supposed to be the most promising refrigerant candidate in heat pump system [5, 6]. In fact, R32 has gained much attention due to its high latent heat, zero ODP, and middle GWP, especially

* Corresponding author, e-mail: junior51020@163.com

in the field of ASHP, and it is expected to replace R410A [7]. However, its high discharge temperature and slight flammability limit its applications in other fields. In order to cover more wide range of air-conditioner, heat pump, and refrigeration systems, refrigerant mixtures R32/R1234ze(E) have attracted great attention in the field of air conditioning and heat pumps due to their excellent properties [8]. Table 1 lists the refrigerants named by the ASHRAE Standard (34-2013) as well as unnamed but widely studied refrigerant mixtures that mainly contain R32 and R1234ze(E) [9]. The zeotropic mixture of R1234ze(E) and R32 with mass fraction of 27/73 which was named L-41b was suggested to be an substitute of R410A in a recent study by AHRI (The Air-Conditioning, Heating, and Refrigeration Institute) [9].

Table 1. List of low GWP refrigerant candidates in Phase I (R410A candidates)

Baseline	Refrigerant	Composition	[Mass%]	Classification	GWP_{100}
R410A	L-41a	R32/R1234yf/ R1234ze(E)	（73/15/12）	A2L	494
	L-41b	R32/ R1234ze(E)	（73/27）	A2L	494
	R32/R134a	R32/ R134a	（95/5）	A2L	713
	R32/R152a	R32/ R152a	（95/5）	A2L	647

Most of the studies available in literatures on the mixture of R1234ze(E) and R32 focused on the thermodynamic properties [10-12], and drop-in replacements in existing refrigeration system [1, 13-16]. In *et al*. [17] presented L-41b drop-in test data of an R410A residential heat pump system. It was found that the drop-in capacities of L-41b systems were 89-94% of those of R410A systems, while that of the COP of L-41b systems were 104-105% of those in R410A systems.

However, flow boiling heat transfer characteristics of the mixture of R1234ze(E) and R32 are rarely reported. Hossaind *et al*. [18] investigated the flow boiling heat transfer characteristics of R1234ze(E) and the mixture of R1234ze(E)/R32 with mass fraction of 55/45 in horizontal tube with inner diameter of 4.35 mm. It is indicated that the local heat transfer coefficients of R1234ze(E)/R32 (mass ratio: 55/45) are slight lower than those of pure R1234ze(E) due to the inferior liquid thermal conductivity and the effect of mass transfer resistance of the mixture.

In this work, we experimentally investigated the local heat transfer coefficients during saturation flow boiling of the mixture L-41b in horizontal tube with an inner diameter of 8 mm. The experimental results were obtained at the saturation temperature of 10 to 20 °C, heat flux ranging from 5-10 kW/m^2, mass flux ranging from 200-500 kg/m^{2}s. Moreover, the experimental heat transfer coefficients are compared with the predicted results obtained by using some empirical prediction models from the literatures, see tab. 5 [19-23]. Additionally, a new vapour-phase multiplier correlation to predict the local heat transfer coefficients of L-41b flow boiling inside smooth tubes is developed based on the model of Choi *et al*.

Experimental set-up

Figure 1 shows the schematic of experimental apparatus in this study. The test fluid is driven by magnetic gear pump and its flow rate is measured by Coriolis effect mass-flow meter. The fluid-flow rate can be adjusted by the electric motor speed by an inverter or bypass-valve installed between inlet and outlet of the gear pump. The refrigerant in the main loop passes through sub-cooler to offset the enthalpy increasing in pump, and to ensure the refrigerant being in sub-cooled condition when it passes through the mass-flow meter.

In front of the test section, a preheater is used to adjust the inlet vapour quality of the test fluid. The heating capacity of the preheater can be adjust by the voltage supply. After that, the refrigerant passes through the test section and condenser, sequentially. Along the test loop, two sight glasses are installed at the inlet and outlet of the test section, allowing to see the two-phase flows. The condenser is installed in a thermostatic bath which consists of a refrigeration system, a heating system and a stirrer. The temperature of thermostatic bath can be adjusted in the range between –20 °C and 30 °C. The test fluid goes back to the liquid reservoir after condensed in the thermostatic bath. The experimental set-up was introduced in detail in the published paper [24].

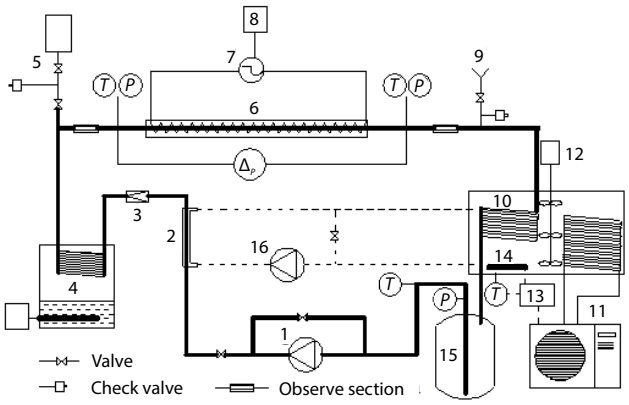

Figure 1. Schematic diagram of the experimental system;
1 – magnetic gear pump, 2 – sub-cooler, 3 – Coriolis mass-flow meter, 4 – preheater, 5 – sampling port, 6 – test section, 7 – electric heater, 8 – electricity meter, 9 – charging port, 10 – condenser, 11 – refrigerating unit, 12 – stirrer, 13 – controller, 14 – heater, 15 – liquid reservoir, 16 – sub-cooler recycle pump

The schematic of the test section is shown on fig. 2. The test tube are made of copper with an inner diameter of 8 mm and a length of 2400 mm. Along the axial of the test tube,

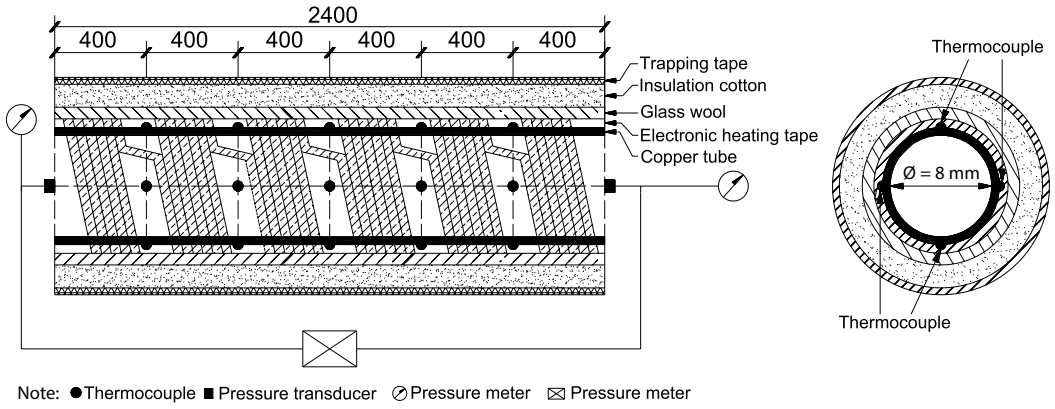

Figure 2. Schematic diagram of the test section

five temperature measuring point are evenly distributed. The wall temperature of each point is measured by the thermocouples embedded in the top, bottom, right and left of the exterior test tube wall. Two pressure transducers are used to measure the inlet and outlet pressures of the test section. The pressure drop between the inlet and the outlet of the test section is measured by a differential pressure transducer. The electric heating tape tightly adhered to the copper surface to generate heat flux as showed in fig. 3. The heat flux in the test section is varied by adjusting the input power of the electric heating tape. In order to reduce heat loss, the test section is insulated by glass wool, insulation cotton and trapping belt. The total heat losing from the test section is estimated to be less than 3.0%.

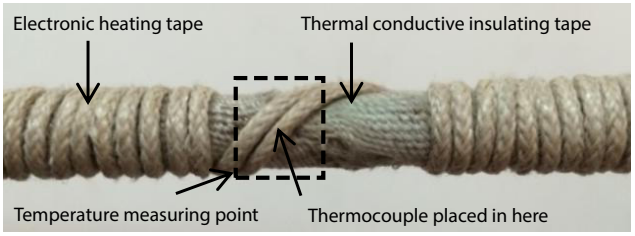

Figure 3. Structure of temperature measuring point in the test section

Data reduction and uncertainty analysis

Data reduction

The local saturation flow boiling heat transfer coefficient is calculated:

$$h_{\mathrm{tp}} = \frac{q}{T_{\mathrm{wi}} - T_{\mathrm{sat}}} \tag{1}$$

$$q = \frac{Q_{\mathrm{test}}}{\pi d_{\mathrm{in}} \Delta z} \tag{2}$$

where q represents the inner wall heat flux of the tube, Q_{test} – the total heat amount in the test section which can be obtained by measuring the total heat input and the heat losses, T_{sat} – the saturation temperature of the fluid, which is determined by the measuring the pressure at the inlet of the test section and the pressure drop along the test section, and T_{wi} – the average inner wall temperature, which can be calculated:

$$T_{\mathrm{wi}} = \frac{1}{20}\sum_{i=1}^{20} T_{\mathrm{wo,i}} - \ln\left(\frac{d_{\mathrm{wo}}}{d_{\mathrm{wi}}}\right)\frac{Q_{\mathrm{test}}}{2\pi\lambda\Delta z} \tag{3}$$

The inlet vapour quality of the test section can be calculated from the energy balance in the test section and the preheater section, which is obtained:

$$i_{\mathrm{test,in}} = X_{\mathrm{in}} i_{\mathrm{test,v,in}} + \left(1 - X_{\mathrm{in}}\right) i_{\mathrm{test,l,in}} \tag{4}$$

$$i_{\mathrm{test,out}} = X_{\mathrm{out}} i_{\mathrm{test,v,out}} + \left(1 - X_{\mathrm{out}}\right) i_{\mathrm{test,l,out}} \tag{5}$$

$$i_{\mathrm{test,in}} = i_{\mathrm{preh,in}} + \frac{Q_{\mathrm{preh}}}{m} \tag{6}$$

$$i_{\mathrm{test,out}} = i_{\mathrm{preh,in}} + \frac{Q_{\mathrm{preh}} + Q_{\mathrm{test}}}{m} \tag{7}$$

where i indicates the specific enthalpy, the subscript *in* and *out* indicate the inlet and outlet of the test section, the subscript v and l indicate the vapour and liquid, Q_{preh} represents the thermal power applied to the preheater, Q_{test} represents the thermal power applied to the test section, m is the flow rate of the test fluid. The average vapour quality is defined:

$$X_{\mathrm{ave}} = \frac{X_{\mathrm{in}} + X_{\mathrm{out}}}{2} \tag{8}$$

The thermodynamic parameters of pure substances are from REFPROP V9.0, Lemon *et al*. [25]. Table 2 summarizes the thermodynamic parameters of the test fluids, which are obtained by using non-ideal mixing rule proposed by Kedzierski *et al.* [26].

Table 2. Thermodynamic parameters of L-41b

Parameters	Unit	T = 283 K	T = 293 K
Molecular weight	[gmol^{-1}]	68.8	68.8
GWP (100 year)	–	493	493
Liquid density	[kgm^{-3}]	1071.2	1034.7
Vapour density	[kgm^{-3}]	26.5	35.9
Liquid thermal conductivity	[mWmK^{-1}]	121.8	107.6
Specific heat	[kJkg^{-1}K^{-1}]	1.678	1.746
Surface tension	[mNm^{-1}]	9.67	8.11
Latent heat	[kJkg^{-1}]	266	251

Uncertainty analysis

All the test parameters were recorded by a data acquisition system when the system reached the steady-state conditions. The temperatures and pressures of the test section were continuously monitored. The criterion for the steady-state conditions was that the variations of the wall and refrigerant saturation temperatures were less than ±0.1 K for 10 minutes. The fluid mass flux was measured by a Coriolis mass-flow meter with an uncertainty of ±1% RS. The power of the preheater was measured by a wattmeter with an uncertainty of ±0.4%. The saturation fluid temperature was measured by the PT 100 Ω resistance thermometer with an uncertainty of ±0.1 °C. The temperature of the out wall was measured by T-type thermocouples with an uncertainty of ±0.1 °C. Table 3 summarizes the measuring ranges and uncertainties of the measurement instruments. The uncertainty analysis was carried out by the method of Moffat [27]. The relative standard uncertainty of heat transfer coefficient can be expressed by the following equation:

$$\frac{u(h)}{h} = \sqrt{\left[\frac{u(q)}{q}\right]^2 + \left[\frac{u(T_{wi})}{T_{wi} - T_{sat}}\right]^2 + \left[\frac{u(T_{sat})}{T_{wi} - T_{sat}}\right]^2} \tag{9}$$

where $u(q)$ is the combined standard uncertainty of heat flux, $u(T_{wi})$ – the combined standard uncertainty of the wall temperature, $u(T_{sat})$ – the combined standard uncertainty of the saturation temperature. Under the operation conditions, the experimental heat transfer coefficients obtained in this work present a minimum value and a maximum value of 2.3% and 12.4%, respectively.

Table 3. Measurement instruments and their uncertainties

Parameters	Instrument	Range	Uncertainty
Refrigerator temperature	PT 100 Ω thermometers	–50200 °C	±0.1 °C
Wall temperature	T-type thermocouple	–20 ~ 100 °C	±0.1 °C
Pressure	Absolute pressure transducer	0 ~ 2MPa	±0.05% FS
Pressure drop	Differential pressure transducer	0 ~ 40kPa	±0.075%
Mass flux	Coriolis mass-flow meter	0.1 ~ 5kg/min	±1%RS
Electricity	Power meter	5 ~ 500V; 0.01 ~ 40 A	±0.4%
Enthalpy	REFPROP V9.0	–	±0.02%

Results and discussion

In the experiment, flow boiling characteristics of L-41b have been investigated under different operation conditions as listed in tab. 4. Then the effects of different parameters on heat transfer coefficient were analysed.

Table 4. Test conditions for the experiment

Mass flux [kgm^{-2}s]	Heat flux [kWm^{-2}]	Quality	Saturation temperature [°C]
200	5.0; 10.0	0.075 ~ 0.785	10±0.5; 20±0.5
300	5.0; 10.0	0.075 ~ 0.785	10±0.5; 20±0.5
400	5.0; 10.0	0.075 ~ 0.785	10±0.5; 20±0.5
500	5.0; 10.0	0.075 ~ 0.785	10±0.5; 20±0.5

Experimental heat transfer coefficients

Figures 4 and 5 show the local heat transfer coefficients of L-41b as a function of vapour quality obtained at saturation temperature of 10.0 ± 0.5 °C and 20.0 ± 0.5 °C with two heat fluxes (5.0 kW/m^2 and 10.0 kW/m^2) and several mass fluxes ranging from 200-500 kg/m^{2}s, respectively. The local heat transfer coefficient of L-41b gradually increases and then decreases with increasing vapour quality.

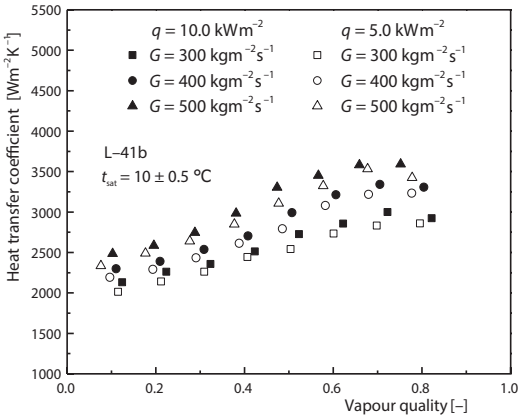

Figure 4. Heat transfer coefficients *vs.* vapour quality (t_{sat} = 10 °C)

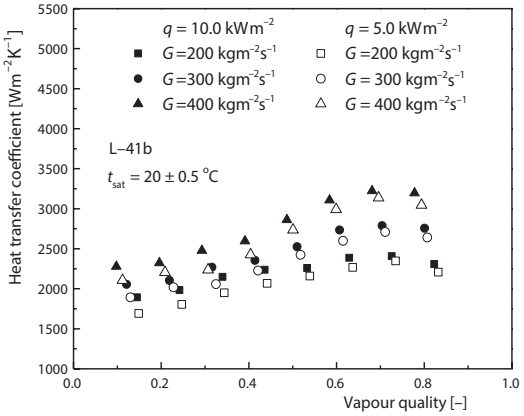

Figure 5. Heat transfer coefficients *vs.* vapour quality (t_{sat} = 20 °C)

The increase of the mass flux leads to a significant enhancement of heat transfer coefficients. This causes a strong increase of the mean fluid velocity during evapouration and a consequent enhancement of the convective boiling contribution. In particular, the ρ_v/ρ_l ratio are about 0.0247 and 0.0367 with the saturation temperature of 10 °C and 20 °C, respectively. This causes a strong increase of the mean fluid velocity during evapouration and a consequent enhancement of the convective boiling contribution. When the mass flux increases from 300-400 kg/m^{2}s, the heat transfer coefficient increase by 9.7% at heat flux of 10.0 kW/m^2 and saturation temperature of 10 °C. when the mass flux increases from 400-500 kg/m^{2}s, the heat transfer coefficient increase by 8.5% at heat flux of 10.0 kW/m^2 and saturation temperature of 10 °C, fig. 6.

The increase of the heat flux leads to a slight increase of the local heat transfer coefficients in the whole range of vapour quality. When the heat flux increases from 5-10.0 kW/m^2, the heat transfer coefficient increase by 4.74% averagely. The heat flux has a stronger effect on the heat transfer coefficients in low vapour quality range than that in high vapour quality due to the dominant nucleate boiling in low vapour quality.

The increase of the saturation temperature leads to a slight decrease of the local heat transfer coefficients in the whole range of vapour quality. The saturation temperature has a stronger effect on the heat transfer coefficients in high vapour quality range than that in low vapour quality. When the saturation temperature increases from 10-20 °C, the heat transfer coefficient increases by 7.52% averagely.

From literatures, it is well accepted that heat transfer coefficient of zeotropic binary mixture is less than the two pure substances because of the concentration gradients. Since the heat transfer degradation of zeotropic mixture L-41b is relatively weak, the heat transfer performance of L-41b is greater than that of R1234ze(E)/R32 (ratio: 55/45) obtained by Hossain *et al*. [18]. Because the heat transfer degradation of R1234ze(E)/R32 (ratio: 55/45) is stronger than that of L-41b due to the difference of temperature glide ($\Delta T_{\text{R1234ze(E)/R32 (ratio: 55/45)}} = 8.9$ °C, $\Delta T_{\text{L-41b}} = 3.1$ °C). Moreover, the main composition of L-41b is R32 with great heat transfer performance as suggested by many researchers.

Predictability verification of exiting correlations to experimental data

In this paper, a comparison of experimental heat transfer coefficients of L-41b with the predicted results using the four empirical correlations is shown in tab. 5 and fig. 7 [19-23]. The absolute average deviation (AAD) and root mean square (RMS) deviation of the correlations and the experimental data are summarized in tab. 6.

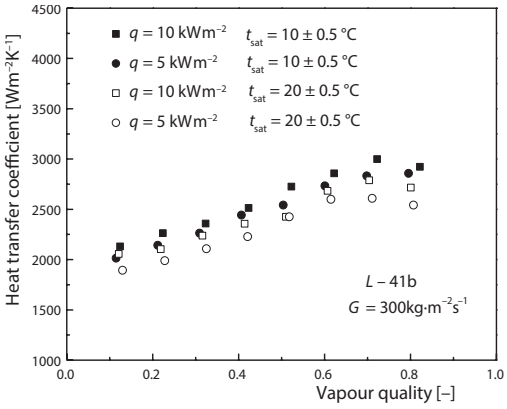

Figure 6. Heat transfer coefficients *vs.* vapour quality at different saturation temperature

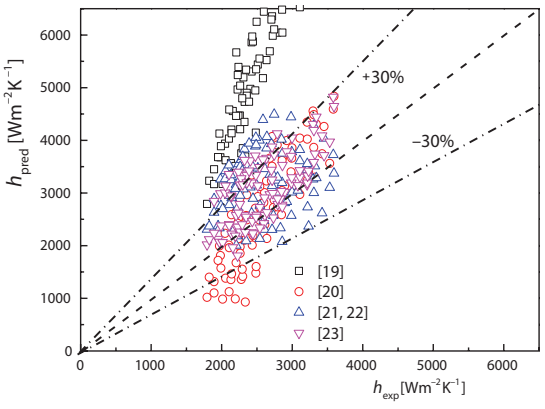

Figure 7. The L-41b experimental data compared with correlation

Among the results, the correlation of Choi *et al*. [20] achieves the best agreement with experimental data. The total AAD is 20.7%. Moreover, approximately 90% of experimental points are within an error bandwidth of ±30% of the prediction. Note that the total AAD obtained with Choi method and Sami method are 20.07% and 20.1%, respectively. Both are acceptable for engineering applications. The correlation (Bivens and Yokozeki [19] and Liu and Winterton [21]) underestimates the measured heat transfer coefficients.

Table 5. Correlation of flow boiling heat transfer coefficient

Bivens and Yokozeki [19]
$h_{tp}=\left[h_{nb}^{2.5}+h_{cv}^{2.5}\right]^{1/2.5}$; $h_{cv}=Fh_lR$; $h_{nb}=55\mathrm{Pr}^{0.12}\left(-\log_{10}\mathrm{Pr}\right)^{-0.55}M_w^{-0.5}q^{n0.67}$; $h_i=0.023\left(\mathrm{Re}_l\right)^{0.8}\left(\mathrm{Pr}_l\right)^{0.4}\left(\frac{\lambda_l}{d}\right)$; $\mathrm{Fr}_l=\frac{G^2}{\rho_l^2gd}$; $h_{tp,m}=h_{tp}/(1+h_{tp}T_{int}q)$; $T_{int}=0.175\Delta t_{bp}\left[1-\exp\left(-q/1.3/10^4/\rho_l/\Delta h_v\right)\right]$; $F=\left[0.29+(1/X_{tt})\right]^{0.85}$; $R=2.15$ when $\mathrm{Fr}_l>0.25$; $R=2.83$ when $\mathrm{Fr}_l\le 0.25$
Correlations of Choi *et al.* [20]
$h_{tp,m}=Eh_{cv}+F_M\mathrm{Sh}_{nb}$; $h_{cv}=0.023\left(\mathrm{Re}_l\right)^{0.8}\left(\mathrm{Pr}_l\right)^{0.4}(\lambda_l/d)$; $E=49.971\mathrm{Bo}^{0.383}X_{tt}^{-0.758}$; $h_{nb}=207(\lambda_l/D_{bl})\left[qD_{bl}/\lambda_lT_{sat}\right]^{0.674}\left(\rho_v/\rho_l\right)^{0.581}\mathrm{Pr}_l^{0.533}$; $S=0.909\mathrm{Co}^{0.301}$; $F_M=\left\{1+0.039\left[C_{p,l}(T_{dew}-T_{bp}/H_{lv})\right]\right\}^{-1}$
Liu and Winterton [21] and Sun *et al.* [22]
$h_{tp,m}=\left[\left(Eh_{cv}\right)^2+\left(F_M\mathrm{Sh}_{nb}\right)^2\right]^{0.5}$; $h_{cv}=0.023\left(\mathrm{Re}_l\right)^{0.8}\left(\mathrm{Pr}_l\right)^{0.4}\left(\lambda_l/d\right)$; $h_{nb}=55\mathrm{Pr}^{0.12}\left(-\log_{10}\mathrm{Pr}\right)^{-0.55}M_w^{-0.5}q_{ch}^{n0.67}$; $E=\left\{1+x\mathrm{Pr}_l\left[(\rho_l/\rho_v)-1\right]\right\}^{0.35}$; $S=\left(1+0.055E^{0.1}\mathrm{Re}_l^{0.16}\right)^{-1}$; $\mathrm{Re}_l=\frac{Gd}{\mu_l}$; $\mathrm{Fh}_l=G^2/(\rho_l^2gd)$; If $\mathrm{Fr}_l\le 0.05$, $E\mathrm{Fr}_l^{0.1-2Fr_l}$ instead of E and $S\mathrm{Fr}_l^{0.5}$ instead of S; $F_M=\left\{1+\Delta T_{bp}/\Delta T_{id}\left|y-x\right|^{c_1}\left(P/10^5\right)^{c_2}\left[1+c_3\exp(-q/3\cdot10^5)\right]\right\}^{-1}$ $c_1=-0.29;c_2=-0.9;c_3=-0.87$
Sami *et al.* [23]
$h_{tp,m}=0.015\lambda_l/d(Gd/\mu_l)^{0.62}A\lambda_l^{0.3}/100$; $A=1-0.79\left[\left\lvert\tilde{y}_1-\tilde{x}_1\right\rvert+\left\lvert\tilde{y}_2-\tilde{x}_2\right\rvert\right]^{0.82}$

Table 6. Deviations between predicted and experimented flow boiling heat transfer coefficient

Saturation temperature [°C]	Heat flux [kW/m²]	Mass flux [kg/m²s]	[19]		[20]		[21]		[23]	
			AAD	*RMS*	*AAD*	*RMS*	*AAD*	*RMS*	*AAD*	*RMS*
10 ± 0.5	10	200	98.73	99.06	27.66	9.45	84.48	73.96	39.37	17.42
		300	107.13	117.56	30.02	10.98	72.83	57.88	42.34	19.97
		400	102.73	108.62	26.67	8.39	59.51	42.03	31.25	13.16
	5	200	106.27	121.71	15.15	3.90	32.26	13.02	10.71	1.34
		300	133.16	191.06	15.69	3.89	30.66	14.06	11.30	1.54
		400	149.75	246.73	16.02	4.81	30.05	14.60	10.24	1.53
20 ± 0.5	10	300	112.87	133.39	23.07	6.40	29.74	13.55	26.97	8.90
		400	122.93	158.10	23.49	6.57	34.55	17.73	26.95	9.14
		500	125.31	164.72	21.94	6.09	37.76	20.65	26.83	8.59
	5	300	141.33	220.17	15.44	5.14	22.31	6.11	4.56	0.30
		400	161.11	285.18	15.41	5.59	28.45	10.46	2.79	0.11
		500	176.98	350.02	17.42	6.81	32.72	13.97	8.40	1.07

Development of a new correlation for L-41b in smooth tubes

Among the results, the correlation of Choi *et al*. [20] achieves the best agreement with experimental data, although, it underestimates the measured heat transfer coefficients in low quality of below 0.3. In the present study, a new correlation will be developed for L-41b in smooth tubes based on Choi model. The heat transfer coefficient is calculated by combining the contributions of the nucleate boiling and forced convective mechanisms by a superposition model:

$$h_{\mathrm{tp}} = Eh_{\mathrm{cv}} + F_M Sh_{\mathrm{nb}} \tag{10}$$

where Eh_{cv} is the contribution of the forced convective mechanism, E – the forced convective heat transfer enhancement factor, and h_{cv} – the calculated from Dittus-Boelter equation:

$$h_{\mathrm{cv}} = 0.023\left(\mathrm{Re_l}\right)^{0.8}\left(\mathrm{Pr_l}\right)^{0.4}\left(\frac{\lambda_{\mathrm{l}}}{d}\right) \tag{11}$$

$$E = C_1 \mathrm{Bo}^{C_2} X_{\mathrm{tt}}^{C_3} \tag{12}$$

where h_{nb} is calculated from Cooper's pool boiling correlation, S – the suppression factor.

$$h_{\mathrm{nb}} = 207\left(\frac{\lambda_{\mathrm{l}}}{D_{\mathrm{bl}}}\right)\left(\frac{qD_{\mathrm{bl}}}{\lambda_{\mathrm{l}}T_{\mathrm{sat}}}\right)^{0.674}\left(\frac{\rho_{\mathrm{v}}}{\rho_{\mathrm{l}}}\right)^{0.581}\mathrm{Pr_l}^{0.533} \tag{13}$$

$$S = C_4 \mathrm{Co}^{C_5} \tag{14}$$

where F_M is the mixture correction factor, which is used to model the mass transfer resistance effect. A correction for F_M is developed based on the experimental data obtained in this work. The values of C_1-C_5 and C_{M} in eq. (16) are empirical constants and obtained by an iteration process to minimize the errors between the heat transfer coefficient calculated from the previous correlations and experimental results. These values are represented in tab. 7. Empirical parameter can be incorporated into correlation for mixtures.

Table 7. Fitting model empirical constant

C_1	C_2	C_3	C_4	C_5	C_{M}
0.272	–0.139	–0.647	2.907×105	0.0244	9.704×105

$$F_M = \left\{1 + C_M\left[\frac{C_{p,\mathrm{l}}\left(T_{\mathrm{dew}} - T_{\mathrm{bp}}\right)}{H_{\mathrm{lv}}}\right]\right\}^{-1} \tag{15}$$

$$h_{\mathrm{tp}} = C_1 \mathrm{Bo}^{C_2} X_{tt}^{C_3} h_{\mathrm{cv}} + C_4 \mathrm{Co}^{C_5}\left[1 + \frac{\left(T_{\mathrm{dew}} - T_{\mathrm{bp}}\right)C_M}{H_{\mathrm{lv}}}\right]^{-1} h_{\mathrm{nb}} \tag{16}$$

Figure 8 presents the comparison of the predicted values of the new correlation with the experimental data. As shown in fig. 8, the deviations of the new correlation are within –24.98% to +14.68% from the experimental data and the 95% prediction values are within ±15%. Therefore, the new correlation can provide good predictions to the flow boiling heat transfer of L-41b inside the 8.0 O. D. horizontal smooth tubes.

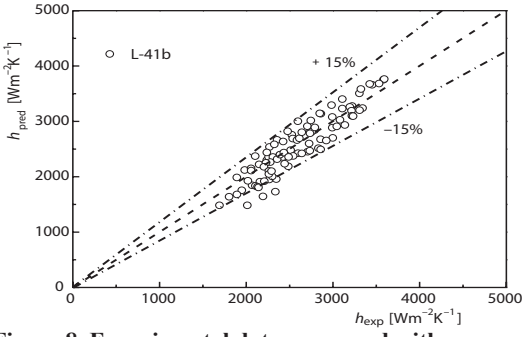

Figure 8. Experimental data compared with correlation

Conclusions

Flow boiling heat transfer characteristics for the binary mixtures of L-41b in a horizontal smooth tube were studied. The influences of saturation, heat flux and mass flux to the heat transfer characteristic were examined and discussed.

The experimental flow boiling heat transfer coefficients were compared with those calculated by the four typical correlations. The correlation of Choi *et al*. [20] achieves the best agreement with experimental data. The total AAD is 20.7%, and approximately 90% of experimental points are in an error bandwidth of ±30% of the prediction.

A modified correlation was developed based on the previous research (Choi *et al*. [20]) and the experimental data in this study. The predicted values from the modified correlation show an acceptable agreement with the experimental data with a relative deviation within –24.98% to +14.68% and the 95% prediction values are within ±15%. Therefore, it can be used to predict the saturated flow boiling heat transfer coefficients of L-41b in horizontal smooth tube.

Acknowledgment

This work was supported by Fujian Education Department Youth Education Technology Project (No. JAT170388) and Scientific Research Foundation of Fujian University of Technology (No. GY-Z160136).

Nomenclature

AAD – absolute average deviation, $[(1/n)\Sigma(|h_{cal} - h_{exp}|/h_{exp})\,]\times100\%$
Bo – Boiling number [$= q/(Gh_{fg})$]
Co – convection number $[\{(1\text{-}x)/x\}^{0.8}(\rho_l/\rho_v)^{0.5}]$
C_p – isobaric specific heat, [$Jkg^{-1}K^{-1}$]
d – tube diameter, [m]
h – heat transfer coefficient, [$kWm^{-2}K^{-1}$]
E – enhancement factor
Fr – Froude number $[=G^2/(\rho^2 gd)]$
g – acceleration of gravity, [ms^{-2}]
G – mass flux, [$kgm^{-2}s^{-1}$]
H_{lv} – latent heat of vaporization, [Jkg^{-1}]
M – molecular weight
P – pressure, [kPa]
Δp – pressure drop, [Pa]
Pr – Prandtl number
Q – heat transfer rate of the whole test section, [Js^{-1}]
q – heat flux, [kWm^{-2}]
Re – Reynolds number
RMS – root mean square deviation, $[(1/n)\Sigma(|h_{cal} - h_{exp}|/h_{exp})^2\,]\times100\%$
S – suppression factor
T – temperature, [K] or [°C]
ΔT – temperature glide, [K] or [°C]
$\tilde{x}$, $\tilde{y}$ – mole fraction of volatile component in liquid and vapour phase, respectively

Greek symbols

ε – void fraction
λ – thermal conductivity, [$Wm^{-1}K^{-1}$]
μ – viscosity, [Pas]
ρ – density, [kgm^{-3}]
σ – surface tension, [Nm^{-1}]

Subscripts

ave – average
cal – calculation
cv – convection
exp – experimental
in – inner
l – liquid
lv – liquid-vapor
nb – nucleate boiling
out – outer
pb – nucleate boiling
pred – predicted
preh – preheater
sat – saturation
v – vapour

References

[1] Adrian, M. B., *et el*., Drop-in Energy Performance Evaluation of R1234yf and R1234ze(E) in a Vapour Compression System as R134a Replacements, *Appl. Therm. Eng.*, *71* (2014), 1, pp. 259-265
[2] Mark, O. M., *et al*., A Thermodynamic Analysis of Refrigerants: Possibilities and Tradeoffs for Low-GWP refrigerants, *Int. J. Refrig.*, *38* (2014), Feb., pp. 80-92

[3] Bhatkar, V. W, *et el*., Alternative Refrigerants in Vapour Compression Refrigeration Cycle for Sustainable Environment: A Review of Recent Research, *Int. J. Environ. Sci. and Tech.*, *10* (2013), 4, pp. 871-880
[4] Bansal. P., *et el*., Advances in Household Appliances – A Review, *Appl. Therm. Eng.*, *31* (2011), 17-18, pp. 3748-3760
[5] Calm, J. M., The Next Generation of Refrigerants Historical Review Consideration and Outlook, *Int. J. Refrig.*, *31* (2008), 7, pp. 1123-1133
[6] Mota-Babiloni, A., *et al*., Refrigerant R32 as Lower GWP Working Fluid in Residential Air Conditioning Systems in Europe and the USA, *Renewable and Sustainable Energy Reviews*, *80* (2017), Dec., pp. 1031-1042
[7] Zilio, C., *et al*., Energy Efficiency of a Reversible Refrigeration Unit Using R410A or R32, *HVAC and R Research*, *21* (2015), 21, pp. 502-514
[8] Mota-Babiloni, A., *et al*., A Review of Refrigerant R1234ze(E) Recent Investigations, *Appl. Therm. Eng.*, *95* (2016), Feb., pp. 211-222
[9] Wang, X., Amrane, K., AHRI Low Global Warming Potential Alternative Refrigerants Evaluation Program (Low-GWP AREP) – Summary of Phase I Testing Results, *Journal of the Taiwan Institute of Chemical Engineers*, *45* (2014), 3, pp. 996-1000
[10] Akasaka, R., Thermodynamic Property Models for the Difluoromethane (R-32)+Trans-1,3,3,3-Tetra- Fluoropropene (R-1234ze(E)) and Difluoromethane+2,3,3,3-Tetrafluoropropene (R-1234yf) Mixtures, *Fluid Phase Equilib.*, *358* (2013), Nov., pp: 98-104
[11] Cui, J., *et al*., Surface Tension and Liquid Viscosity of R32+R1234yf and R32+R1234ze, *Journal Chem. and Eng. Data*, *61* (2016), 2, pp. 950-957
[12] Jia, T., *et al*., Volumetric Properties of Binary Mixtures of Difluoromethane (R32) + Trans-1,3,3,3-Tetra-Fluoropropene (R1234ze(E)) at Temperatures from 283.15 K to 363.15 K and Pressures up to 100 MPa, *Journal Chem. Thermodynamics*, *101* (2016), Oct., pp. 54-63
[13] Cheng, Z., *et al*., Numerical Research on R32/R1234ze(E) Air Source Heat Pump under Variable Mass Concentration, *Int. J. Refrig.*, *82* (2017), Oct., pp. 1-10
[14] Lee, H., *et al.*, LCCP Evaluation on Various Vapour Compression Cycle Options and Low GWP Refrigerants, *Int. J. Refrig.*, *70* (2016), Oct., pp. 128-137
[15] Moles, F., *et al*., Theoretical Energy Performance Evaluation of Different Single Stage Vapour Compression Refrigeration Configurations Using R1234yf and R1234ze(E) as Working fluids, *Int. J. Refrig.*, *44* (2014), Aug., pp. 141-150
[16] Adrian, M. B., *et al*., Theoretical Comparison of Low GWP Alternatives for Different Refrigeration Configurations Taking R404A as Baseline, *Int. J. Refrig*., *44* (2014), Aug., pp. 81-90
[17] In, S., *et al*., Performance Test of Residential Heat Pump after Partial Optimization Using Low GWP Refrigerants, *Appl. Therm. Eng.*, *72* (2014), 2, pp. 315-322
[18] Hossain, M. A., *et al*., Heat Transfer during Evaporation of R1234ze(E), R32, R410A and a Mixture of R1234ze(E) and R32 Inside a Horizontal Smooth Tube, *Int. J. Refrig.*, *36* (2013), 2, pp. 465-477
[19] Bivens, D. L., A. Yokozeki, A., Heat Transfer Coefficients and Transport Properties for Alternative Refrigerants, *Proceeding*, International Refrigeration Conference, Purdue, Id, USA, 1994, pp. 299-304
[20] Choi, T. Y., *et al*., Evapouration Heat Transfer of R-32, R-134a, R-32/R-134a, and R-32/125/134a Inside a Horizontal Smooth Tube, *Int. J. Heat and Mass Trans.*, *43* (2000), 19, pp. 3651-3660
[21] Liu, Z., Winterton, R. H .S., A General Correlation for Saturated and Subcooled Flow Boiling in Tubes and Annuli, Based on a Nucleate Pool Boiling Equation, *Int. J. Heat Mass Trans.*, *34* (1991), 11, pp. 2759-2766
[22] Sun, Z., *et al*., Nucleate Pool Boiling Heat Transfer Coefficients of Pure HFC134a, HC290, HC600a, and their Binary and Ternary Mixtures, *Int. J. Heat and Mass Trans.*, *50* (2007), 1-2, pp. 94-104
[23] Sami, S. M., *et al.*, Prediction of the Heat Transfer Characteristics of R22/R152a/R114 and R22/R152a/R124, *ASHRAE Trans.*, *98* (1992), Part 2, pp. 51-58
[24] Qiu, J., *et al*., Experimental Investigation of Flow Boiling Heat Transfer and Pressure Drops Characteristic of R1234ze(E), R600a, and a Mixture of R1234ze(E)/R32 in a Horizontal Smooth Tube, *Advances in Mechanical Engineering*, *7* (2015), 9, pp. 1-12
[25] Lemmon *et al*., NIST Reference Fluid Thermodynamic and Transport Properties Database (REFPROP), Version 10, National Institute of Stadards and Technology (NIST), Applied Chemicals and Materials Division, Boulder, Col., USA

[26] Kedzierski, A., *et al.*, Cause of the Apparent Heat Transfer Degradation for Refrigerant Mixtures, *ASME HTD Two-Phase Flow and Heat Trans.*, *197* (1992), Aug., pp. 149-158
[27] Moffat, R. J., Describing the Uncertainties in Experimental Results, *Exp. Therm. Fluid*, *1* (1988), 1, pp. 3-17

Paper submitted: January 15, 2018
Paper revised: May 9, 2018
Paper accepted: May 13, 2018